Title 40 CFR Part 191
Compliance Certification
Application
for the
Waste Isolation Pilot Plant

MASS Attachment 4-1

THIS PAGE INTENTIONALLY LEFT BLANK

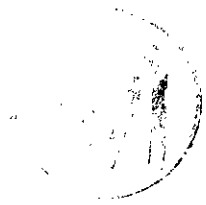

WFO 30840

INFORMATION ONLY

FEP Screening Analysis

S1: Verification of 2D-Radial Flaring Using 3D Geometry

WBS No. 1.1.6.3 [At time work was initiated, May 1995]

SWCF-A: 1.2.07.3: PA:QA:TSK: S1

ERRATA - February 19, 1996

Palmer Vaughn
Lead Staff Member: Palmer Vaughn
Sandia National Laboratories
Organization 6749

Contributors:

Teklu Hadgu, Ecodynamics Research Associates
David McArthur, Sandia National Laboratories, Org. 6514
James Schreiber, Science Applications International Corporation

S-1: Verification of 2-D WIPP PA Grid Using 3-D Geometry
Summary Memo of Record

TO: D. R. Anderson

FROM: P. Vaughn

SUBJECT: FEP Screening Issue S-1

DATE: January 26, 1996

STATEMENT OF SCREENING DECISION

FEP Screening Issue S-1 need not be included in future system-level performance assessment calculations.

STATEMENT OF SCREENING ISSUE

The present 2-D WIPP PA grid and lumping of rooms and panels used in the performance assessment (PA) conceptual model need to be justified by comparison to a more detailed representation of the repository, shafts, and surrounding Salado Formation including repository dip. Concerns regarding the current conceptualization include the following:

Results using a 2-D WIPP PA grid need to be compared to those for a 3-D model to establish the reliability of the simplification for identical geometric conditions. This comparison should be performed for a consistent representation of the repository in both cases with the only change being the dimensionality of the model. When dip is included, the problem becomes fully three-dimensional, and the 2-D WIPP PA grid option becomes much more questionable. With the 2-D WIPP PA grid, brine and gas flows are required to occur laterally in the entire element, whereas they may actually only occur in a very limited section.

The objective of the current study is thus to test the performance and adequacy of the 2-D grid by comparing it with a 3-D grid constructed based on the 2-D model.

APPROACH

The first task was construction of a conceptual model to be used for the study. The 2-D PA grid was constructed from a 3-D conceptualization in which rooms, panels, and drifts were first lumped together to form a much-simplified 3-D repository geometry. The 2-D grid is a further simplification that is intended to preserve accessible pore volume. The method is described in detail in Chapter 4 of Volume 4 of the Preliminary Performance Assessment (1992). Construction of the 3-D grid for this study started from the simplified 3-D repository geometry, and the third (east-west) dimension was gridded instead of being lumped into two dimensions.

Currently, the 2-D mesh being used for WIPP Performance Assessment calculations consists of 31 grid blocks in the x-axis and 27 grid blocks in the vertical axis for a total of 837 grid blocks. If we add a third dimension with, say, 31 grid blocks, the total number of blocks in 3-D will be 25,947. This gridding size would require computation times that are prohibitive. Therefore, in order to reduce the size of the problem, and to concentrate on the regions of importance, some simplifications were adopted:

- To concentrate on the repository and waste, the Rustler and Castile formations, and all formations above the Rustler were excluded. Thus the grid includes only the Salado formation.

- Because of symmetry in the north-south-direction, only one half of the problem was considered.

- In the actual repository, connections between the panels are through the seals. Thus, any other connections between the single panel and the rest of the repository were removed. The same procedure was applied to the experimental and operations regions.

The above simplifications do not invalidate the study because all regions of importance to the implementation of the performance measures were included.

A new model of the WIPP site was developed for the current study based on the simplifications described above. The model retains the features of the original grid but some grid blocks are lumped together. These simplifications resulted in reducing the total number of 3-D grid blocks to 2100 (*i.e.*, NX = 21, NZ = 10, NY = 10 for the TOUGH28W run, and NX = 23, NY = 12, NZ = 10 for the 3-D BRAGFLO runs). This modified 3-D grid runs at a reasonable speed for the purpose of the current study. Note that the computation times would still be unreasonable for routine probabilistic runs (see Table 2, Appendix 2 for a comparison of CPU times). Results will be compared with a similarly modified 2-D grid.

After construction of the simplified 2-D and 3-D grids, simulation procedures, as used for the compliance Performance Assessment were conducted. The TOUGH28W code, which is a WIPP version of the code TOUGH2 (Pruess, 1991), was used for the 3-D simulation, and BRAGFLO was used for both 2-D and 3-D simulations. Since TOUGH28W does not currently have the capacity to model gas generation and brine consumption, gas generation was modeled as a constant average source value over the repository. Brine consumption was not included in the simulations. The simulations calculated flow in the WIPP site for a period of 10, 000 years starting from -5 years, the same as in the PA calculations. At -5 years, the WIPP site is at hydrostatic condition except for the excavated regions, which are at 1 atm. pressure. The first 5 years of the simulation (-5 to 0) represent the operational period of the repository, during which some depressurization and brine drainage occurs in the formations surrounding the repository. At time 0, the waste material is placed in the repository, and creep-closure and gas generation are activated. At 100 years, shaft seal material properties are changed. At 1000 years, the intrusion well is activated, and gas generation is stopped. The disturbed option (intrusion well scenario) was selected because it is associated with higher releases to the environment, compared to the undisturbed option. For the current study gas generation is stopped at 1000 years, which means that the maximum pressure for both disturbed and undisturbed scenarios would be the same.

Median values were input for distributed parameters. The simulation was based on two cases of gas generation rates in the repository. The rates were based on the estimated repository gas generation of 1600 moles per drum, reported on page A-11 of Volume 3 of the Preliminary Performance Assessment (1992), and 3200 moles per drum to account for other sources such as plastics and rubber as potential gas generators. The first case (*i.e.*, the base case) used an average gas generation rate in the repository of 1.6 moles per drum per year for 1000 years. The second case used a gas generation rate double that of the first case. The higher rate would include potential gas generation due to plastics and rubber. It will also allow fracturing of the anhydrite layers so that the effect of dip and fracturing on flow were included. Note that all runs included the 1-degree dip.

The results of simulation were to be compared based on the performance measures. The selected performance measures include pressure in the repository (because it is important for blowout and fracturing), and brine out flow at the top of shaft, top of the intrusion well and at the 2.4 km land withdrawal boundary.

RESULTS AND DISCUSSION

A simplified version of the two dimensional WIPP PA grid being used for WIPP PA has been tested against a corresponding three dimensional model. BRAGFLO was used for both 2-D and 3-D simulations, and TOUGH28W was used for the 3-D simulations only. Simulation results were compared for cases with an average repository gas generation rate, and a gas generation rate double the average gas generation rate. The simulation results were plotted and are shown in Figs. 6 to 16 in Appendix 2. The results of Case 2 (*i.e.*, doubled gas generation rate) indicate that a combination of pressure induced fracturing and the 1-degree dip cause flow paths which are different for the 2-D and 3-D grids. Once fracturing occurs, the 3-D model displays an immediate migration of gas primarily out of the west side of the repository into the anhydrite layers, accompanied by brine inflow to the repository. This phenomenon is not seen in the results from the 2-D model, in which the west side of the repository is a no-flow boundary

(see Figs. 12 and 15), which demonstrates that the 2-D and 3-D simulations show local variations. However the results also show that predictions of brine flow to the accessible environment are similar for both grids. The main advantage of the 2-D grid over the 3-D grid is the reduced computation time and storage, allowing an efficient and fast processing of data for the numerous vectors that are required for the probabilistic Performance Assessment calculations. Following is a summarized analysis of the results based on the selected performance measures:

- The amount of brine inflow and outflow at the 2.4 km boundary of the anhydrite layers is low. For Case 1 (*i.e.*, median gas generation rate), the cumulative inflow over the 10,000-year performance period for 2-D BRAGFLO was about 800 kg (0.65 m^3), and outflow was about 400 kg (0.33 m^3). The corresponding 3-D BRAGFLO results show an inflow of about 15,400 kg (12.5 m^3) and outflow of 114 kg (0.093 m^3) at the boundary. For Case 2 (*i.e.*, doubled gas generation rate) the cumulative inflow over 10,000 years for 2-D BRAGFLO was 0.3 kg (2.4 x 10^{-4} m^3), and the cumulative outflow was 8411 kg (6.8 m^3). The corresponding 3-D BRAGFLO results were a cumulative inflow of 15383 kg (12.5 m^3) and a cumulative outflow of 817 kg (0.66 m^3). For both Case 1 and Case 2, the 2-D BRAGFLO results are consistently higher than those of the 3-D. Note that these figures represent only half of the repository, and that the amount of contamination of the brine has not been verified.

- Both 2-D and 3-D results showed that at the top of the shaft there was no brine flow out, but some gas flowed out.

- Both 2-D and 3-D showed that there was no brine flow from panel up the borehole following intrusion.

- The results of repository pressure for both 2-D and 3-D with TOUGH28W and BRAGFLO were in good agreement. Plots for the base gas generation rate shown in Fig. 6 are almost identical. Plots for the doubled gas generation rate (see Fig. 11) are also identical except at the peak, where some differences occur.

BASIS FOR RECOMMENDED SCREENING DECISION

Comparison of outputs of calculations of the simplified 2-D WIPP PA grid and a corresponding 3-D grid, based on the selected input data, showed that results were equivalent for the most part. Although the 3-D grid showed flow details which were not accurately represented with the 2-D grid, the computed releases to the accessible environment for both grids were nearly equivalent. This indicates that, based on the performance measures and the overall uncertainty, the current model being used for WIPP Performance Assessment is sufficient for estimates of calculated releases. Calculations using the 2-D grid are more computationally efficient, which is necessary for the large number of vectors.

CERTIFICATION AND TRAINING

The following individuals were responsible for the calculations and analysis of the FEP screening effort:

T. Hadgu, D. McArthur and J. Schreiber.

Head staff member and reviewers included:

M. Lord, R. MacKinnon and P. Vaughn.

Copies of certification and training of personnel involved in the FEP screening issue S-1 are on file in the SWCF. All staff were trained on QAP's.

CORRESPONDENCE

None

REFERENCES

Butcher, B. M., S. W. Webb, and J. W. Berglund, 1995. *System Prioritization Method-Iteration 2. Baseline Position Paper: Disposal Room and Cuttings Models, Volume 2*, Appendix F. March 28, 1995. Albuquerque, NM: Sandia National Laboratories.

Christian-Frear, T. and Webb, T., 1995. Milestone SH001: Preliminary Comparison of BRAGFLO and TOUGH28W using a WIPP PA Specific Conceptual Model for Undisturbed Conditions.

International Formulation Committee, 1967. *A formulation of the Thermodynamic Properties of Ordinary Water Substance*, IFC Secretariat, Düsseldorf, Germany.

Pruess, K., 1983. *Development of a General Purpose Simulator MULKOM, Annual Report 1982*, Earth Sciences Division, report LBL-15500, Lawrence Berkeley Laboratory.

Pruess, K., 1987. *TOUGH Users' Guide*, Report LBL-20700, Lawrence Berkeley Laboratory, CA.

Pruess, K., 1991. *TOUGH2-A General-Purpose Numerical Simulator for Multiphase Fluid and Heat Flow*, Report LBL-29400, Lawrence Berkeley Laboratory, CA.

WIPP PA (Performance Assessment) Department, 1992. *Preliminary Performance Assessment for the Waste Isolation Pilot Plant, December 1992-Volume 4: Uncertainty and Sensitivity Analyses for 40 CFR 191, Subpart B*, SAND92-0700/4, Albuquerque, NM: Sandia National Laboratories.

WIPP PA (Performance Assessment) Department, 1992. *Preliminary Performance Assessment for the Waste Isolation Pilot Plant, December 1992-Volume 3: Model Parameters*, SAND92-0700/3, Albuquerque, NM: Sandia National Laboratories.

WIPP PA (Performance Assessment) Department, 1995. *User's Manual for BRAGFLO, Version 3.62ZO*, Albuquerque, NM: Sandia National Laboratories.

WIPP PA (Performance Assessment) Department, 1995. *Software Quality Assurance Notebook for BRAGFLO, Version 3.62ZO*, Albuquerque, NM: Sandia National Laboratories.

APPENDIX 1: Overview of BRAGFLO and TOUGH28W

As stated earlier, both BRAGFLO and TOUGH28W were used to simulate flow in the repository site. Note that the verification of BRAGFLO for QA included comparing output of BRAGFLO with that of TOUGH2 and with analytical solutions of selected problems (see Software Quality Assurance Notebook for BRAGFLO, 1995). In addition, Christian-Frear and Webb (1995) compared results of BRAGFLO and TOUGH28W using a WIPP model with median values for an undisturbed scenario. Both the QA verification work and the comparison of the codes using the WIPP model showed that results of the two codes were very similar. Because of those findings a decision was made to use both codes for the present study. However, it should be pointed out that although both codes solve the same equations of motion, code architecture, solution methods, some fluid properties are not the same. A list of some of the differences is given below.

BRAGFLO is the numerical simulator being used for WIPP PA to study flow in the repository site. It is a two-phase (brine and gas), isothermal finite difference simulator which uses mass balance equations and Darcy's law. The non-linear equations are solved using the Newton-Raphson iterative scheme, and a direct equation solver. The code includes WIPP-specific processes such as pressure induced fracturing, creep closure, gas generation and brine consumption.

TOUGH28W is the WIPP version of TOUGH2 (*i.e.*, TOUGH2 with EOS8) which includes WIPP-specific processes such as pressure induced fracturing and creep closure. TOUGH2 (Pruess, 1991) is a non-isothermal, multiphase flow integral finite difference numerical simulator for porous and fractured media. It assumes Darcy flow. TOUGH2 and the earlier version TOUGH (Pruess, 1987) belong to the MULKOM family of codes (Pruess, 1983). The coupled non-linear equations are solved using the Newton-Raphson iterative scheme, and the code allows a selection of direct and preconditioned conjugate gradient solvers. TOUGH2 includes a number of equation of state (EOS) modules to evaluate fluid properties of different fluids.

Following is a list of some features and differences of the two codes. Note that these differences are as of the present, and that both codes could be modified to include new features.

- BRAGFLO uses brine pressure and gas saturation as primary variables for two-phase flow. The initial conditions in the input require brine saturation. TOUGH28W uses gas pressure, gas saturation and temperature as primary variables, and requires gas saturation initially.

- BRAGFLO uses finite differences while TOUGH28W uses integral finite differences to approximate the partial differential equations of motion. TOUGH28W does not depend on any global coordinate system. However, for the problem at hand, the two methods are equivalent since Cartesian geometry is used.

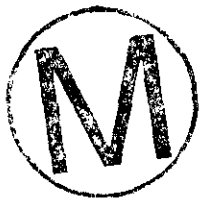

- BRAGFLO uses a direct equation solver with LU-decomposition. TOUGH28W has a selection of direct and preconditioned conjugate gradient (pcg) solvers. The pcg solvers require less storage and are normally expected to be faster than direct solvers, and so are useful for large problems. In this study, BRAGFLO with its direct solver turned out to be faster by a factor of 4.

- The convergence criteria, tolerances and time step controls are different in the two codes. BRAGFLO uses individual Newton-Raphson convergence criteria for pressure and saturation. TOUGH28W requires separate convergence criteria and tolerance limits for Newton-Raphson and the preconditioned conjugate gradient solvers. In TOUGH28W convergence of Newton-Raphson iterations depends on a general criterion (size of residual), rather than on individual primary variables, as in BRAGFLO.

- There are differences in the evaluation of interface parameters for flow calculation. BRAGFLO employs harmonic averaging of permeabilities, densities, viscosities and interface areas, and upstream weighting of relative permeabilities. TOUGH28W gives the user a choice of weighting methods. For the current simulations options that are close to those of BRAGFLO were selected.

The selected options were upstream weighting of relative permeabilities and viscosity, harmonic weighting of permeability, and arithmetic averaging of density.

- TOUGH28W uses a formatted input which requires input information placed at specified position. BRAGFLO uses unformatted input. The input of BRAGFLO allows simulations to continue to 10,000 years without stopping to change input parameters at selected times. TOUGH28W, on the other hand, needs to be stopped when material properties have to be changed (such as when shaft seal permeability is changed at 100 years).

- BRAGFLO has a set of input and output data processing codes and plotting capabilities. This allows a vastly more efficient analysis of data than currently is available on TOUGH28W. Similar codes have been developed for TOUGH2 but are not available to all users.

- Both codes allow pressure induced fracturing of the anhydrite layers. But the input parameters for fracturing are not the same. For instance, TOUGH28W requires changes in pressure above initial pressure for both initiation and ending of fracturing. In the case of BRAGFLO, the corresponding input parameters are change in pressure above initial pressure for initiation of fracturing, and change of pressure above the initiation pressure for ending fracturing. Note that the setup in TOUGH28W needs modification. Currently, when restarting is done after change of input parameters, the initial pressures are not stored, resulting in new initial pressures. This needs to be changed.

- Both codes allow for creep closure of the excavated areas. Currently, both use data generated by SANTOS (Butcher *et al.*, 1995) based on studies of salt creep. The tabulated data are in the form of Pressure-Time relations, and are used to modify formation porosity. Simulations show that the creep closure option in TOUGH28W slows calculations significantly. Modifications might be required so that the computation speed is improved.

- BRAGFLO computes gas generation and brine consumption due to corrosion and biodegradation. Currently this option is not fully functional on TOUGH28W.

- For capillary pressure and Klinkenberg effect BRAGFLO requires input of individual constants while TOUGH28W uses a combination of the constants. For instance, in the correlation for formation permeability to gas: $k_g = k_w(1 + bk_w^{-a} / p)$, BRAGFLO requires the values of the constants a and b as input while TOUGH28W requires the term bk_w^{-a}. In the case of capillary pressure, the input to TOUGH28W is residual liquid saturation, residual gas saturation, parameter lambda, threshold pressure and maximum pressure. The input to BRAGFLO is the same as the above except for threshold pressure. In BRAGFLO, the threshold pressure is calculated as a function of permeability using: $P_t = a\,k^h$, and the constants a and h are the input parameters. Input parameters are selected so that the sub-models are equivalent in treatment.

- BRAGFLO uses the Redlich-Kwong-Soave equation of state to evaluate gas density. Brine density is calculated based on a constant fluid compressibility. Both gas and liquid viscosities are assumed constant and are required as input. TOUGH28W uses the perfect gas law for gas density. Brine density and liquid and gas viscosities are all dependent on temperature and pressure. Properties of water are obtained from the steam table equations of the International Formulation Committee (1967). To facilitate comparisons with BRAGFLO the equation of brine density used in BRAGFLO has been added to TOUGH28W.

It should be pointed out that comparisons between BRAGFLO and TOUGH2 (commercial version), using selected problems for the verification BRAGFLO, showed similar results (see Software Quality Assurance Notebook for BRAGFLO, 1995).

APPENDIX 2: Discussion of Results

Following is a discussion of results of FEP S-1 for the 2-D and 3-D grids for Cases 1 and 2 using BRAGFLO and TOUGH28W computer codes. CPU times and time steps are given in Table 2.

Case 1: Base Gas Generation Rate

Results of simulation for Case 1 are shown in Figs. 6 to 10. The figures show plots of average gas pressure, gas saturation and porosity in the repository (*i.e.*, Materials 17 and 19 in Figs. 1 and 2); gas mass in place in the repository; cumulative net brine inflow into the repository and cumulative brine outflow from the repository. The plots are results of 2-D and 3-D BRAGFLO, and 3-D TOUGH28W. For Case 1, the pressures were not high enough to cause pressure induced fracturing in the anhydrite layers. The results are mostly in general agreement, as is shown in the figures. The curves for average gas pressure and porosity in the repository (Figs. 6 and 8, respectively) are almost identical. Initially the repository is at atmospheric pressure. As brine flows into the excavated regions, and also due to the generation of gas in the repository, the pressure increases (Fig. 6). At 1000 years, the intrusion well penetrates the repository, which allows gas to escape. As a result the pressure drops. The three curves show almost identical behavior.

Fig. 7 shows simulation results for average gas saturation in the repository. The curves show a similar trend. At time zero, brine continues to flow into the excavated region due to differences in hydrostatic head. Although gas is generated at this time, the effect of the hydrostatic head is more important. In addition, gas escapes through the shaft, as the shaft seal is not placed yet. Thus the gas saturation drops initially. At 100 years, the shaft seal is placed, and the gas saturation stabilizes up to 1000 years. At 1000 years, gas generation is stopped, and gas starts to escape through the intrusion well. In addition, brine flows into the repository. This causes gradual decline of the gas saturation until it drops to its residual value. Note that exactly the same trend is not followed in the individual grid blocks, and that the curves only show average behavior. The three curves are close until about 1500 years but differ in the period 1500 - 7000 years. These differences are also shown in plots of cumulative net brine inflow into the repository (Fig. 10). As shown in Figs. 7 and 10, the plots for 3-D BRAGFLO and 3-D TOUGH28W are closer to one another than to 2-D BRAGFLO. For instance, both curves show full brine saturation at about 8800 years while the prediction of 2-D BRAGFLO is at about 9500 years. Thus these differences may be attributed to differences in prediction of 2-D and 3-D grids. The differences between the 3-D BRAGFLO and TOUGH28W are believed to be due to the differences in the two codes described in Appendix 1.

Fig. 9 shows gas mass in place in the repository. Again, all curves show the same trend. The mass in place increases between 100 and 1000 years due to gas generation. It then drops drastically due to gas withdrawal through the intrusion well and because gas generation is discontinued. The mass in place continues to drop gradually until the immobile quantity is reached. The predictions are slightly different around the peak mass in place, which is probably due to differences in the equations of gas density, among other reasons.

Fig. 10 shows plots of brine net inflow and outflow at the repository. The calculations are based on flow through all boundaries of the Panel and Rest of Repository (see Figs. 1 and 2). Note that a plot of outflow for 3-D TOUGH28W has not been provided because the method of evaluation of the outflow was not the same as in BRAGFLO. 2-D BRAGFLO predicts a maximum outflow of about 3×10^6 kg (2439 m^3) while 3-D BRAGFLO predicts about 4.3×10^6 kg (3496 m^3) at 10,000 years. Fig. 15 shows the corresponding plots for the doubled gas generation case. In the plot, 2-D BRAGFLO predicts maximum brine outflow of about 2×10^6 kg (1626 m^3) whereas 3-D BRAGFLO predicts a slightly higher value of about 2.5×10^6 kg (2032 m^3) at 10,000 years. This potentially contaminated brine flows to the DRZ, where it mixes with a large volume of uncontaminated brine. Some of this mixture of uncontaminated and potentially contaminated brine migrates to the anhydrite layers (mainly to MB139). The amount of brine flow to the halite which has a very low permeability is not significant. The extent to which the brine is contaminated is not known from the BRAGFLO calculations alone. In any case the brine outflow at the 2.4 km anhydrite boundary is very low for both 2-D and 3-D, as shown above. Note also that the calculations did not include brine consumption in the waste due to chemical reactions (*i.e.*, because TOUGH28W did not have this option). According to earlier work, a large portion of the brine inflow to the repository is consumed. Thus the calculations of brine outflow from the repository would have been much lower if brine consumption was included.

One of the reasons for the differences observed in the predictions of the 2-D and 3-D curves is the method of weighting of inter-block parameters. For instance, the flow areas between grid blocks in the 3-D cases are the same while those of the 2-D model are different. Thus, when BRAGFLO applies harmonic weighting on the areas the magnitude of the flux will be different from that of the 3-D cases.

Case 2: Doubled Gas Generation Rate

For this case the gas generation rate of Case 1 was doubled. The objective of this case was to include contributions of gas generation due to plastics and rubber, and also to allow fracturing in the anhydrite layers in order to study its effect on the performance of the 2-D approximation. Doubling the gas generation allowed pressures to build-up and cause pressure induced fracturing in the anhydrite layers. Note that our earlier attempt was to include TOUGH28W for Case 2 calculations. As stated in Appendix 1, currently TOUGH28W does not store initial conditions at time 0, which are required for the pressure induced fracturing model. Thus TOUGH28W could only be used if restarting is avoided. In our attempt to use TOUGH28W we decided to make shaft seal property changes at time 0 (instead of at 100 years), and run 0 - 1000 years without any restarting. Thus, all Case 2 calculations do not have shaft seal property changes at 100 years. Everything else, except for gas generation rate, remained as in Case 1. The above modifications could allow TOUGH28W to run to 1000 years. However since another restarting is required at 1000 years, it was finally decided not to use TOUGH28W for Case 2. Only results of 2-D and 3-D BRAGFLO are compared for this case. Results of simulation are shown in Figs. 11 to 16.

Fig. 11 shows plots of gas pressure vs. time for 2-D and 3-D BRAGFLO. Because of doubling the gas generation rate, the maximum pressure in this case is over 17 MPa for 2-D BRAGFLO compared to 12.5 MPa in Case 1. This caused fracturing in the anhydrite layers, as is evident from the permeability changes observed. The predictions of gas pressure in the repository are nearly the same except at the peak. 2-D BRAGFLO predicts a maximum of about 17.5 MPa while 3-D predicts about 16.5 MPa. In this case, the shaft seal is installed at time zero (as opposed to 100 years for Case 1) and thus gas build-up starts early.

Fig. 12 shows plots of gas saturation. In this case a sharp drop is observed in the predictions of 3-D BRAGFLO earlier than in Case 1. In Case 1 the drop occurred at 1000 years, because the intrusion well penetrated the repository, and gas generation was stopped. In Case 2, in addition to the reasons given for Case 1, fracturing in the anhydrite layers causes the gas saturation to drop. Results of permeability changes demonstrate that fracturing occurs before 1000 years, which explains the drops in saturation shown in Fig. 12. On the other hand, 2-D BRAGFLO shows a gradual drop of saturation, although fracturing has occurred.

The sharp drop in saturation is in line with changes in cumulative net brine inflow into the repository (Fig. 15), and porosity in the anhydrite layers (Fig. 16). This is due to a combination of pressure induced fracturing and the 1-degree dip. A study of the 3-D results shows significant permeability increases in the North-West section of the anhydrite layers. This causes an increased migration of gas out of the repository, which in turn induces an inflow of brine into the repository (see Fig. 15). Note that the maximum fracturing occurs up-dip where the maximum changes in pressure occur. Although 2-D BRAGFLO predicts fracturing in the anhydrite layers, the magnitude of average porosity and permeability changes are different from 3-D (see Fig. 16). In addition, fracturing for 3-D is spread over the 3-D geometry whereas fracturing for 2-D occurs to the south and north only. As a result, changes in saturation and mass movement are not as sharp. Since gas saturation is stopped and the intrusion well is introduced at 1000 years, the effect of fracturing is reduced in the time beyond 1000 years. Once the effect of fracturing subsides the predictions of the two models are similar, which is why the curves are parallel in Figs. 12 and 15. Note that in Case 2 the repository is not brine saturated at 10,000 years.

Fig. 16 shows plots of volume averaged porosity for 2-D and 3-D BRAGFLO. Grid block porosities in all anhydrite layers were volume averaged in the region bounded by the 2.4 km land withdrawal boundary. This analysis may be used as a measure of the fracture porosity enhancement. Note that the analysis is over all anhydrite layers and that local variations were not reported. The extent of fracturing for 2-D is similar to that of 3-D along the North-South axis. For materials MB139 and Anhydrite A and B the fracturing extends to the first anhydrite grid block past the excavated region both in up-dip and down-dip directions. For material MB138, the fracturing extends to the first anhydrite grid block in the down-dip direction, and to two grid blocks in the up-dip direction. In the East-West direction fracturing in the 3-D grid extends over one grid block, except near the North-West corner of the excavated area where more fracturing is observed.

Table 1: Material Properties at Different Simulation Periods

-5 to 0 Years

					Modified Brooks-Corey Parameters				
Material Name	Permeability (m^2)	Porosity	Compres. (1/Pa)	Klinkenberg Factor (MPa)	Lambda	Resid. Liquid Saturation	Resid. Gas Saturation	Threshold Pressure (Pa)	Maximum Cap. Pressure (Pa)
S-HALITE 12	1.E-21	0.01	8.054E-9	8.341E+0	0.7	0.3	0.2	9.e6	1.E+8
DRZ_1 16	1.E-15	0.01	8.279E-8	8.734E-2	0.7	0.0	0.0	0.0	1.E+24
TRANS_1 14	1.E-15	0.01	8.279E-8	8.734E-2	0.7	0.0	0.0	0.0	1.E+24
S_MB138 13	2.51E-19	0.019	4.121E-9	1.347E+0	0.7	0.2	0.165	0.0	1.E+24
S_ANH_AB 15	2.51E-19	0.019	4.121E-9	1.347E+0	0.7	0.2	0.165	0.0	1.E+24
S_MB139 22	2.51E-19	0.019	4.121E-9	1.347E+0	0.7	0.2	0.2	0.0	1.E+24
SHFT_B_1 2	1.E-10	1.0	0.0	8.938E-3	0.7	0.0	0.0	0.0	1.E+8
SHFT_LS1 4	1.E-10	1.0	0.0	8.938E-3	0.7	0.0	0.0	0.0	1.E+8
REPOSIT 17	1.E-10	1.0	0.0	5.067E-3	0.7	0.0	0.0	0.0	1.E+24
PANEL 19	1.E-10	1.0	0.0	5.067E-3	0.7	0.0	0.0	0.0	1.E+24
BACKFILL 20	1.E-10	1.0	0.0	8.938E-3	0.7	0.0	0.0	0.0	1.E+24
EXP_AREA 21	1.E-10	1.0	0.0	8.938E-3	0.7	0.0	0.0	0.0	1.E+24

0 to 100 Years

					Modified Brooks-Corey Parameters				
Material Name	Permeability (m^2)	Porosity	Compres. (1/Pa)	Klinkenberg Factor (MPa)	Lambda	Resid. Liquid Saturation	Resid. Gas Saturation	Threshold Pressure (Pa)	Maximum Cap. Pressure (Pa)
S-HALITE 12	1.E-21	0.01	8.054E-9	8.341E+0	0.7	0.3	0.2	9.e6	1.E+8
DRZ_1 16	1.E-15	0.01	8.279E-8	8.734E-2	0.7	0.0	0.0	0.0	1.E+24
TRANS_1 14	1.E-15	0.01	8.279E-8	8.734E-2	0.7	0.0	0.0	0.0	1.E+24
S_MB138 13	2.51E-19	0.019	4.121E-9	1.347E+0	0.7	0.2	0.165	0.0	1.E+24
S_ANH_AB 15	2.51E-19	0.019	4.121E-9	1.347E+0	0.7	0.2	0.165	0.0	1.E+24
S_MB139 22	2.51E-19	0.019	4.121E-9	1.347E+0	0.7	0.2	0.165	0.0	1.E+24
SHFT_B_1 2	1.E-12	0.075	1.333E-8	8.938E-3	0.7	0.2	0.2	7.947E+03	1.E+8
SHFT_LS1 4	1.E-12	0.050	1.2E-8	8.938E-3	0.7	0.2	0.2	4.268E+05	1.E+8
REPOSIT 17	5.585E-12	0.6602	0.0	5.067E-3	0.7	0.2	0.2	0.0	1.E+24
PANEL 19	5.585E-12	0.6602	0.0	5.067E-3	0.7	0.2	0.2	0.0	1.E+24
BACKFILL 20	1.E-12	0.075	0.0	8.938E-3	0.7	0.0	0.0	0.0	1.E+24
EXP_AREA 21	1.E-12	0.075	0.0	8.938E-3	0.7	0.0	0.0	0.0	1.E+24

EPA TP 2-19-96

100 to 1000 Years

Modified Brooks-Corey Parameters

Material Name		Permeabiliy (m^2)	Porosity	Compres. (1/Pa)	Klinkenberg Factor (MPa)	Lambda	Resid. Liquid Saturation	Resid. Gas Saturation	Threshold Pressure (Pa)	Maximum Cap. Pressure (Pa)
S-HALITE	12	1.E-21	0.01	8.054E-9	8.341E+0	0.7	0.3	0.2	9.e6	1.E+8
DRZ_1	16	1.E-15	0.01	8.279E-8	8.734E-2	0.7	0.0	0.0	0.0	1.E+24
TRANS_1	14	1.E-15	0.01	8.279E-8	8.734E-2	0.7	0.0	0.0	0.0	1.E+24
S_MB138	13	2.51E-19	0.019	4.121E-9	1.347E+0	0.7	0.2	0.165	0.0	1.E+24
S_ANH_AB	15	2.51E-19	0.019	4.121E-9	1.347E+0	0.7	0.2	0.165	0.0	1.E+24
S_MB139	22	2.51E-19	0.019	4.121E-9	1.347E+0	0.7	0.2	0.165	0.0	1.E+24
SHFT_B_1	2	1.E-12	0.075	1.333E-8	8.938E-3	0.7	0.2	0.2	7.947E+03	1.E+8
SHFT_LS1	4	1.E-17	0.050	1.2E-8	3.992E-1	0.7	0.2	0.2	4.268E+05	1.E+8
REPOSIT	17	5.585E-12	0.6602	0.0	5.067E-3	0.7	0.2	0.2	0.0	1.E+24
PANEL	19	5.585E-12	0.6602	0.0	5.067E-3	0.7	0.2	0.2	0.0	1.E+24
BACKFILL	20	1.E-12	0.075	0.0	8.938E-3	0.7	0.0	0.0	0.0	1.E+24
EXP_AREA	21	1.E-12	0.075	0.0	8.938E-3	0.7	0.0	0.0	0.0	1.E+24

ERRATA
2-19-96

1000 to 10,000 Years

Modified Brooks-Corey Parameters

Material Name		Permeabiliy (m^2)	Porosity	Compres. (1/Pa)	Klinkenberg Factor (MPa)	Lambda	Resid. Liquid Saturation	Resid. Gas Saturation	Threshold Pressure (Pa)	Maximum Cap. Pressure (Pa)
S-HALITE	12	1.E-21	0.01	8.054E-9	8.341E+0	0.7	0.3	0.2	9.e6	1.E+8
DRZ_1	16	1.E-15	0.01	8.279E-8	8.734E-2	0.7	0.0	0.0	0.0	1.E+24
TRANS_1	14	1.E-15	0.01	8.279E-8	8.734E-2	0.7	0.0	0.0	0.0	1.E+24
S_MB138	13	2.51E-19	0.019	4.121E-9	1.347E+0	0.7	0.2	0.165	0.0	1.E+24
S_ANH_AB	15	2.51E-19	0.019	4.121E-9	1.347E+0	0.7	0.2	0.165	0.0	1.E+24
S_MB139	22	2.51E-19	0.019	4.121E-9	1.347E+0	0.7	0.2	0.165	0.0	1.E+24
SHFT_B_1	2	1.E-12	0.075	1.333E-8	8.938E-3	0.7	0.2	0.2	7.947E+03	1.E+8
SHFT_LS1	4	1.E-17	0.050	1.2E-8	3.992E-1	0.7	0.2	0.2	4.268E+05	1.E+8
REPOSIT	17	5.585E-12	0.6602	0.0	5.067E-3	0.7	0.2	0.2	0.0	1.E+24
PANEL	19	5.585E-12	0.6602	0.0	5.067E-3	0.7	0.2	0.2	0.0	1.E+24
BACKFILL	20	1.E-12	0.075	0.0	8.938E-3	0.7	0.0	0.0	0.0	1.E+24
EXP_AREA	21	1.E-12	0.075	0.0	8.938E-3	0.7	0.0	0.0	0.0	1.E+24
WELL		3.161E-13	0.37	0.0	1.307E-2	0.7	0.2	0.0	0.0	1.E+24

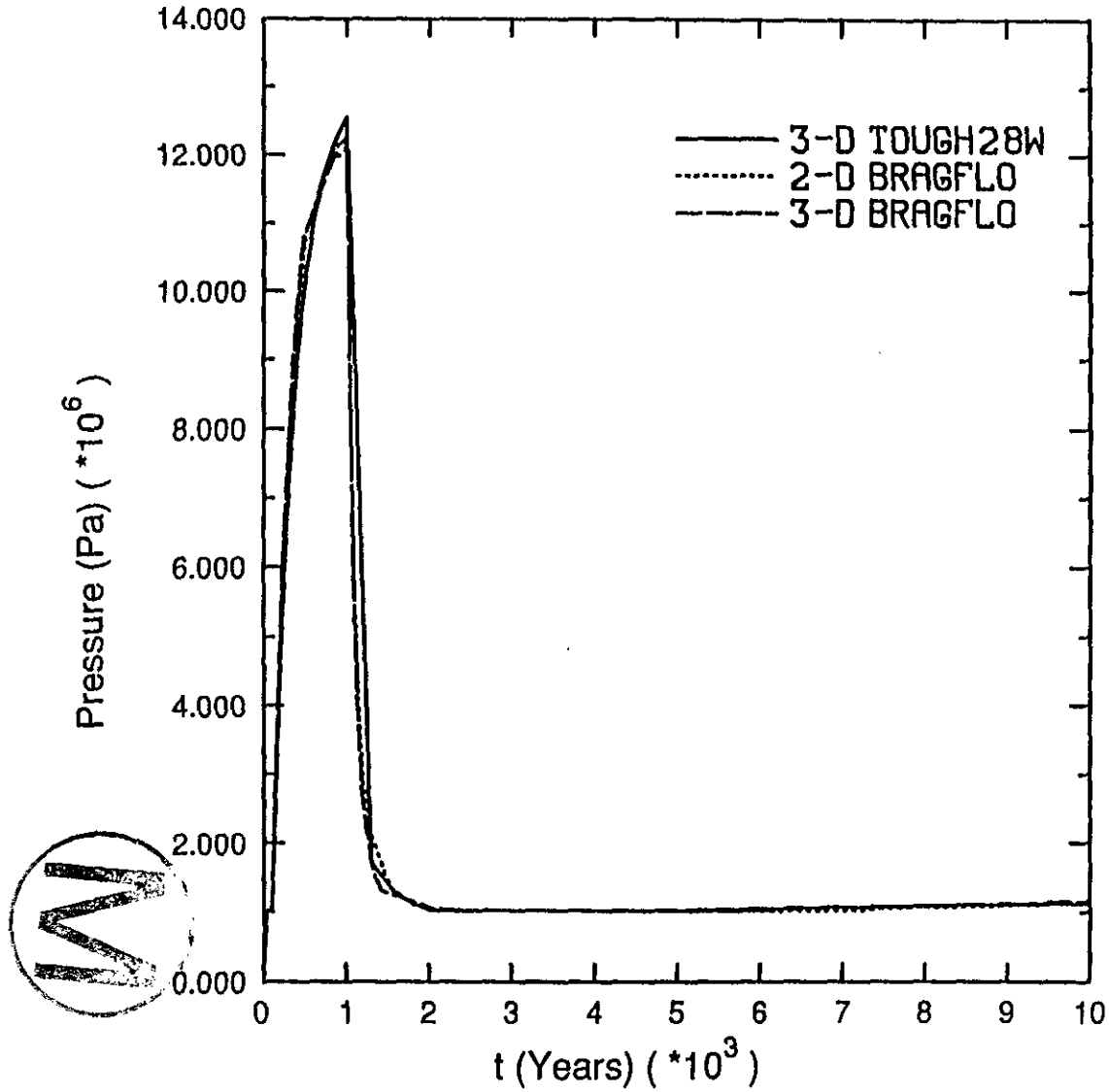

Fig. 6 Average Pressure in Repository - Base Gas Generation rate

ERRATA
2-19-96

SPLAT X2.0 01/24/96 17:21:22

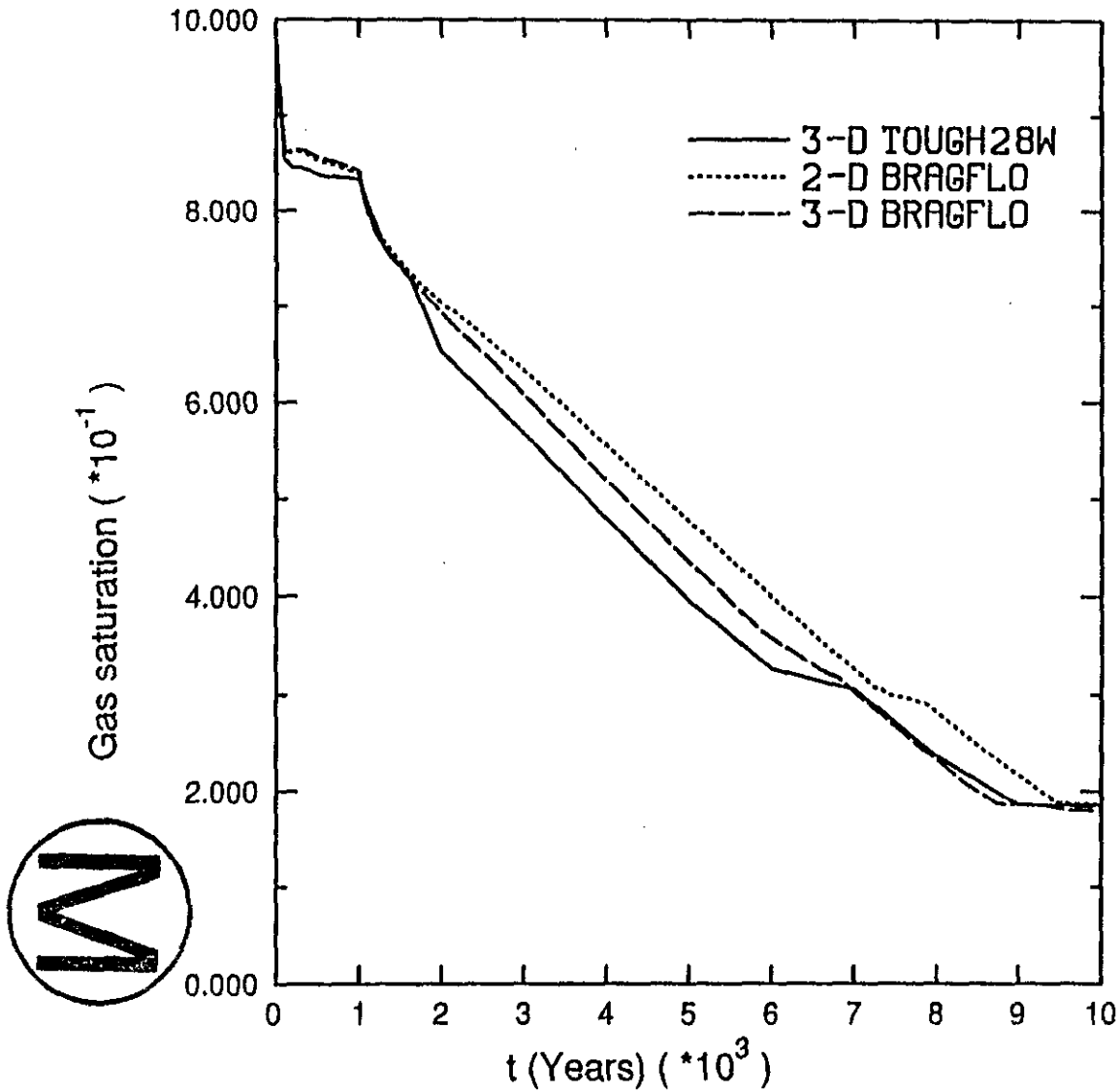

Fig. 7 Average Gas Saturation in Repository - Base Gas Generation rate

SPLAT X2.0 01/24/96 17.28 06

ERRATA 2-19-96

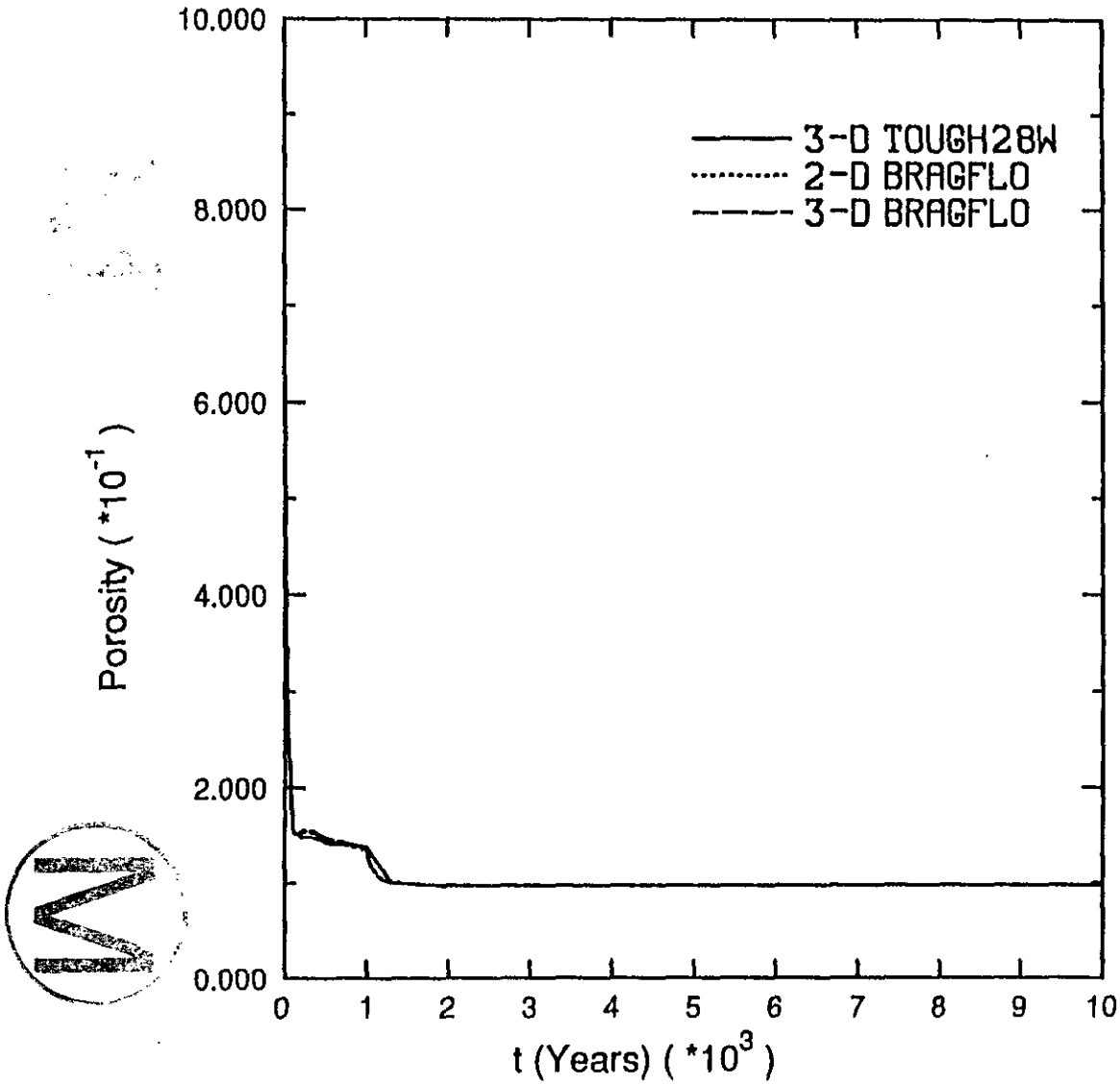

Fig. 8 Average Porosity in Repository - Base Gas Generation rate

SPLAT X2.0 01/24/96 17:30:14

CREATA 3-19-96

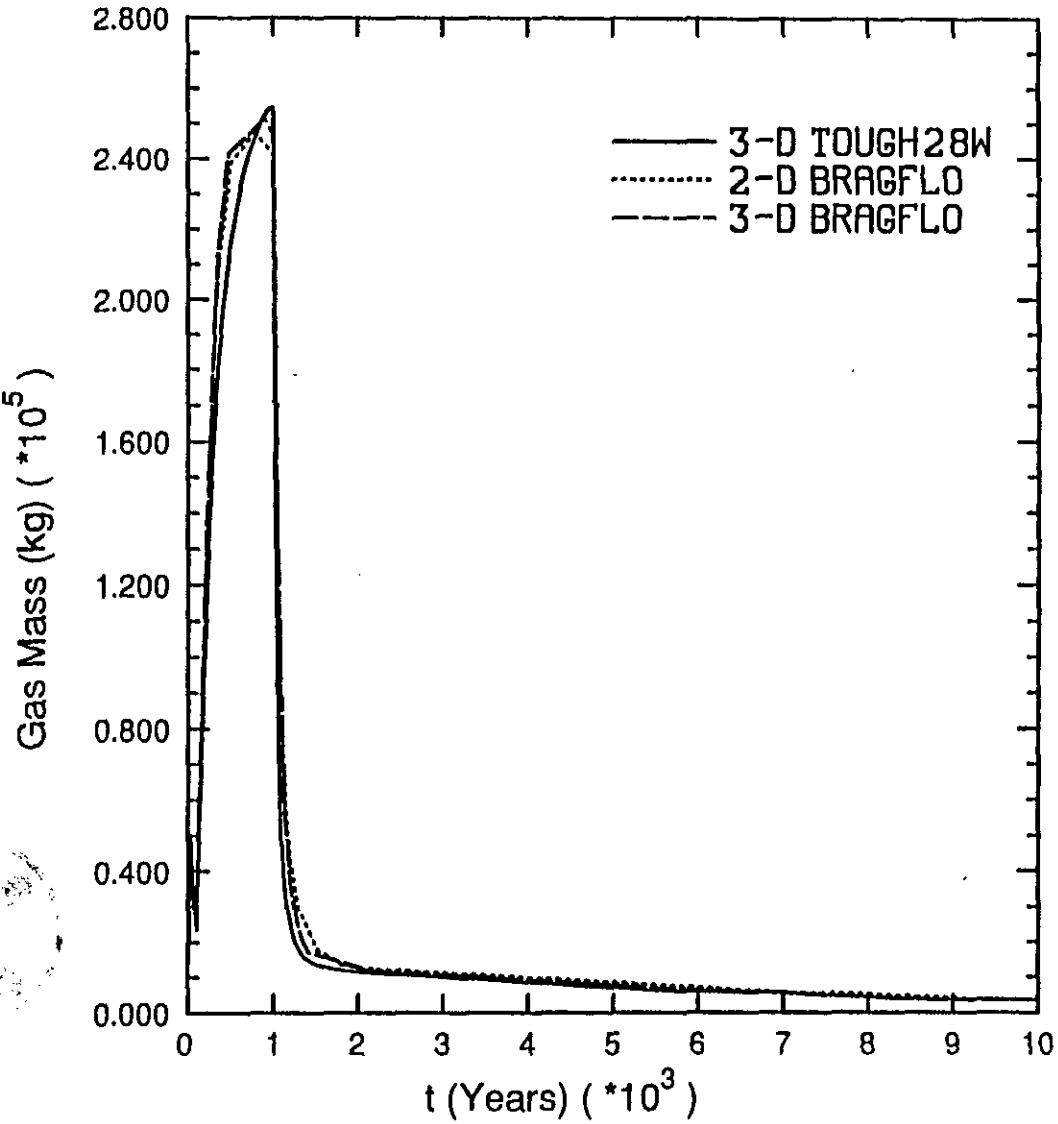

Fig. 9 Gas Mass in Place in Repository - Base Gas Generation rate

SPLAT X2.0 01/24/96 17:43.02

ERRATA 2-19-96

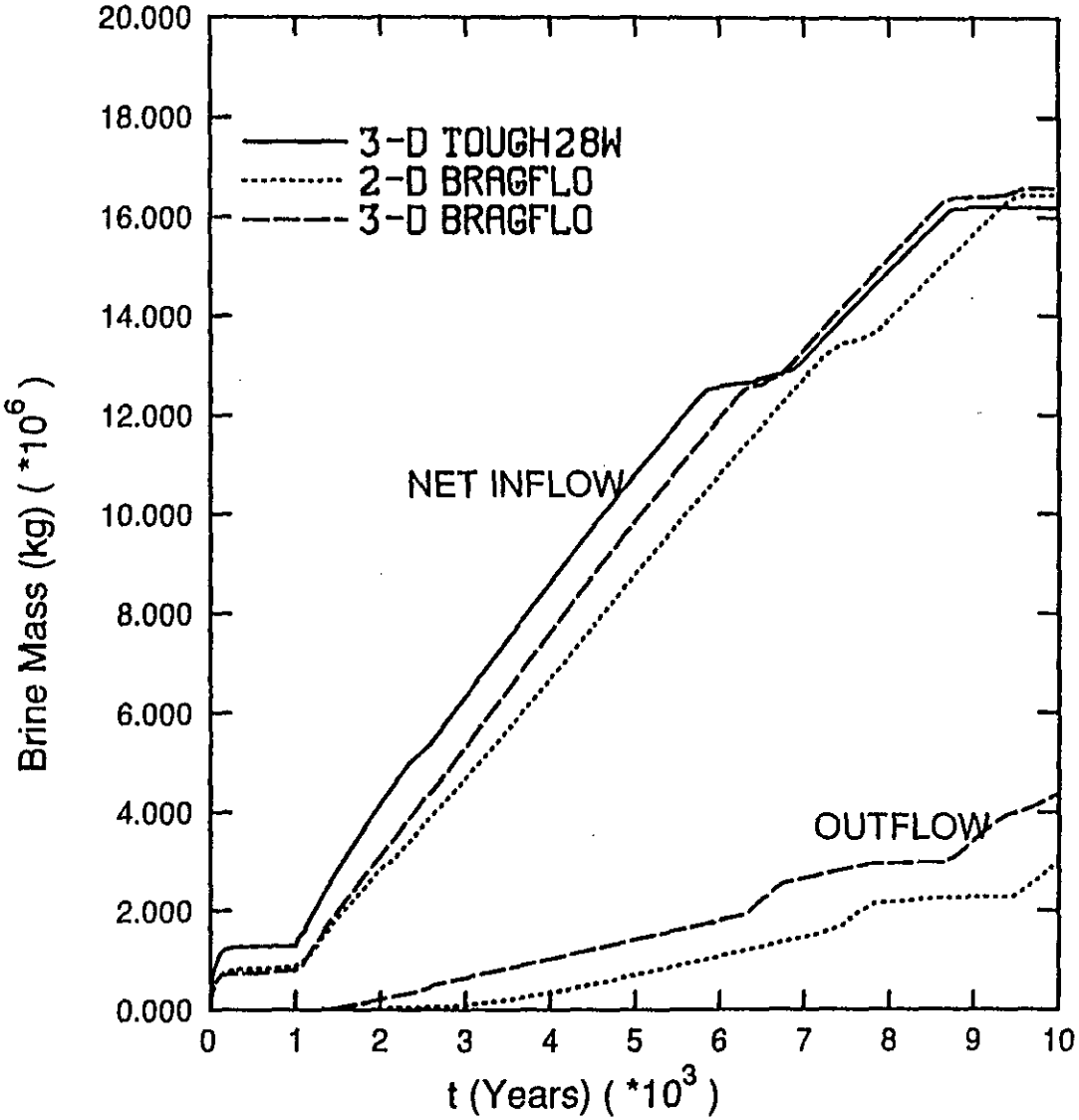

Fig. 10 Cumulative Net Brine In and Outflow at Repo. - Base Gas Generation rate

SPLAT X2.0 01/24/96

ERRATA 2-19-96

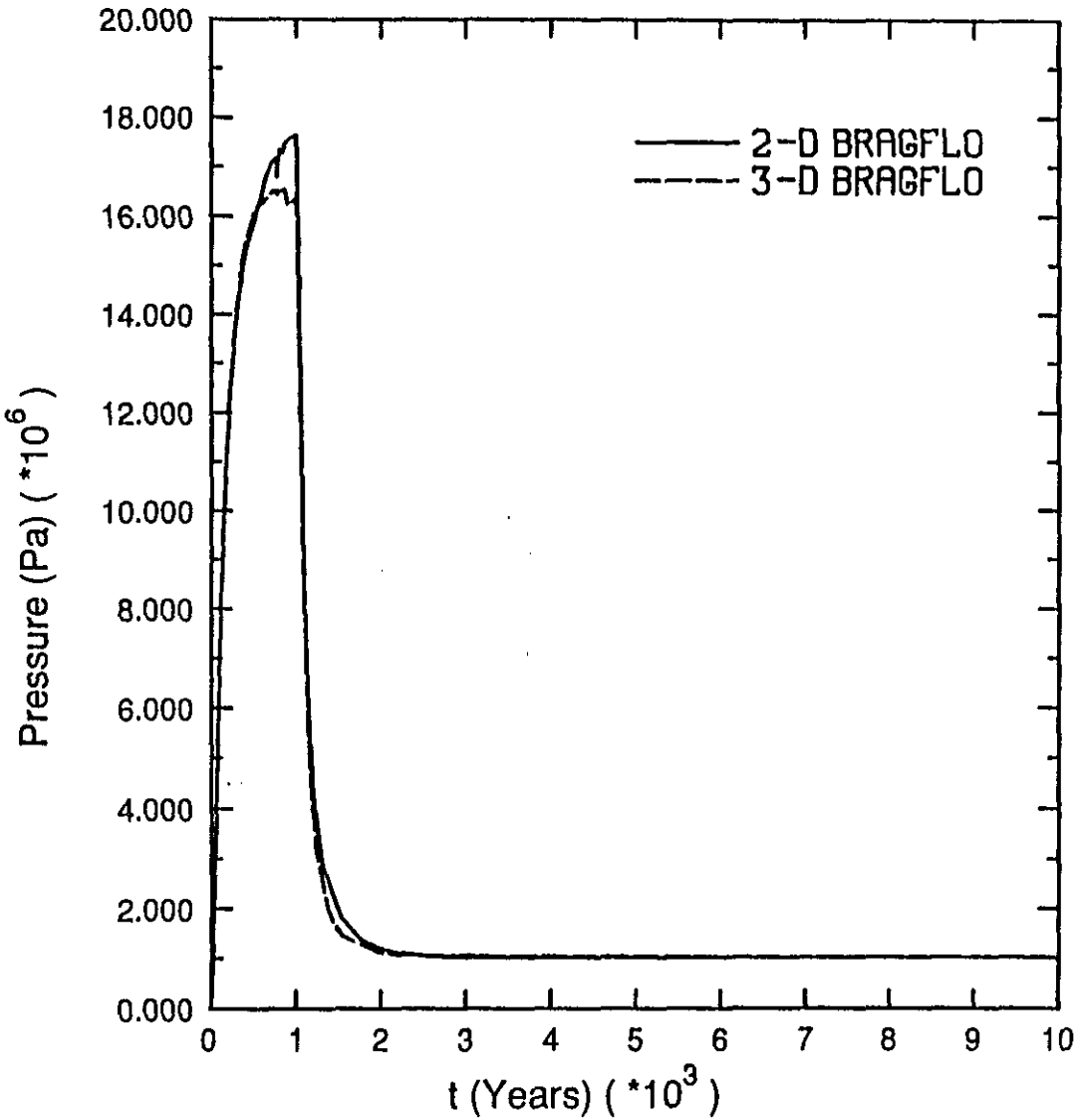

Fig. 11 Average Pressure in Repository - Doubled Gas Generation rate

SPLAT X2.0 01/24/96 18:39:06

ERRATA
2-19-96

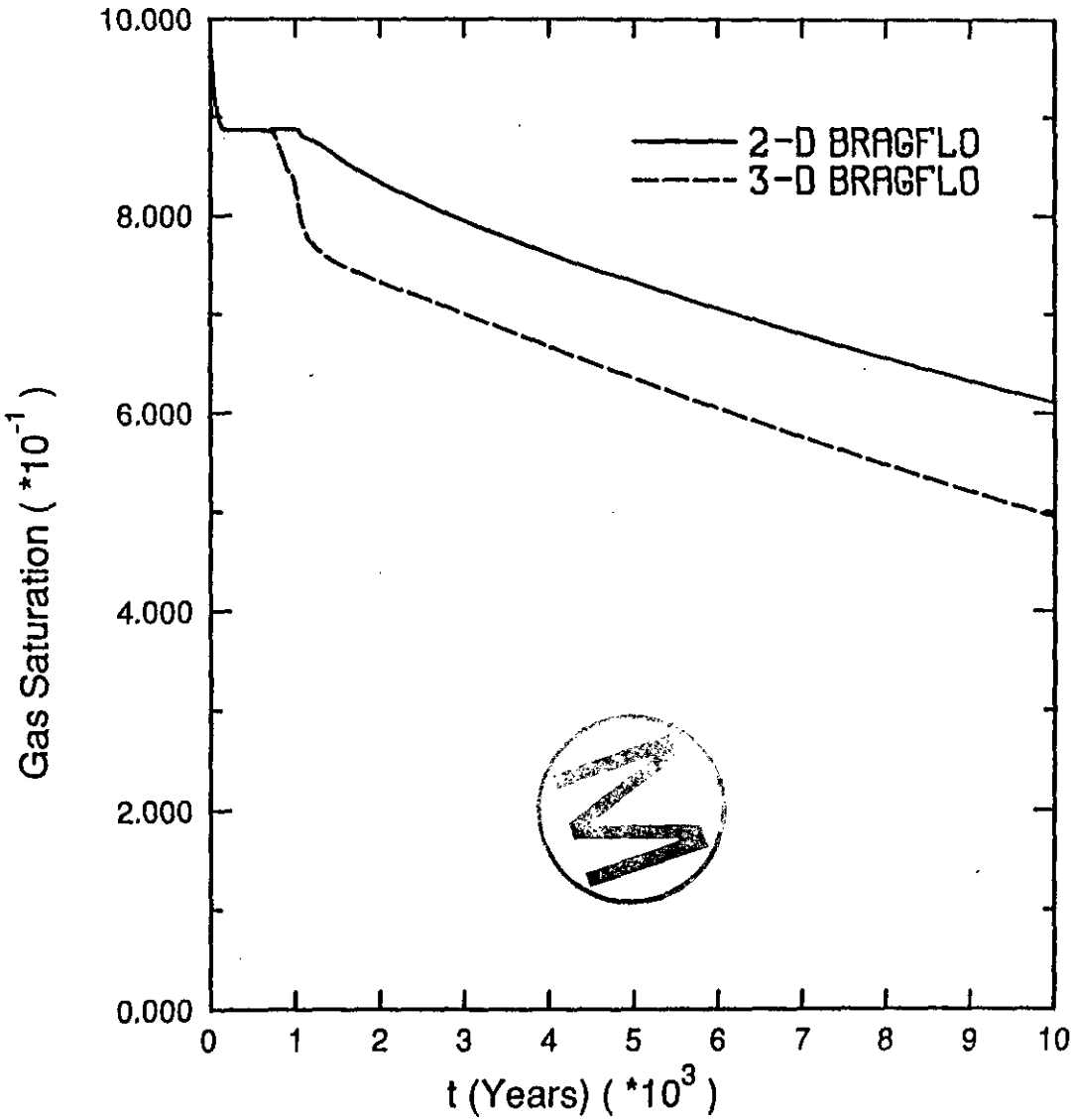

Fig. 12 Average Gas Saturation in Repository - Doubled Gas Generation rate

ERRATA 2-19-96

SWCF-A:1.2.07.3:PA:QA:TSK:S1

32

SPLAT X2.0 01/24/96 18:45:03

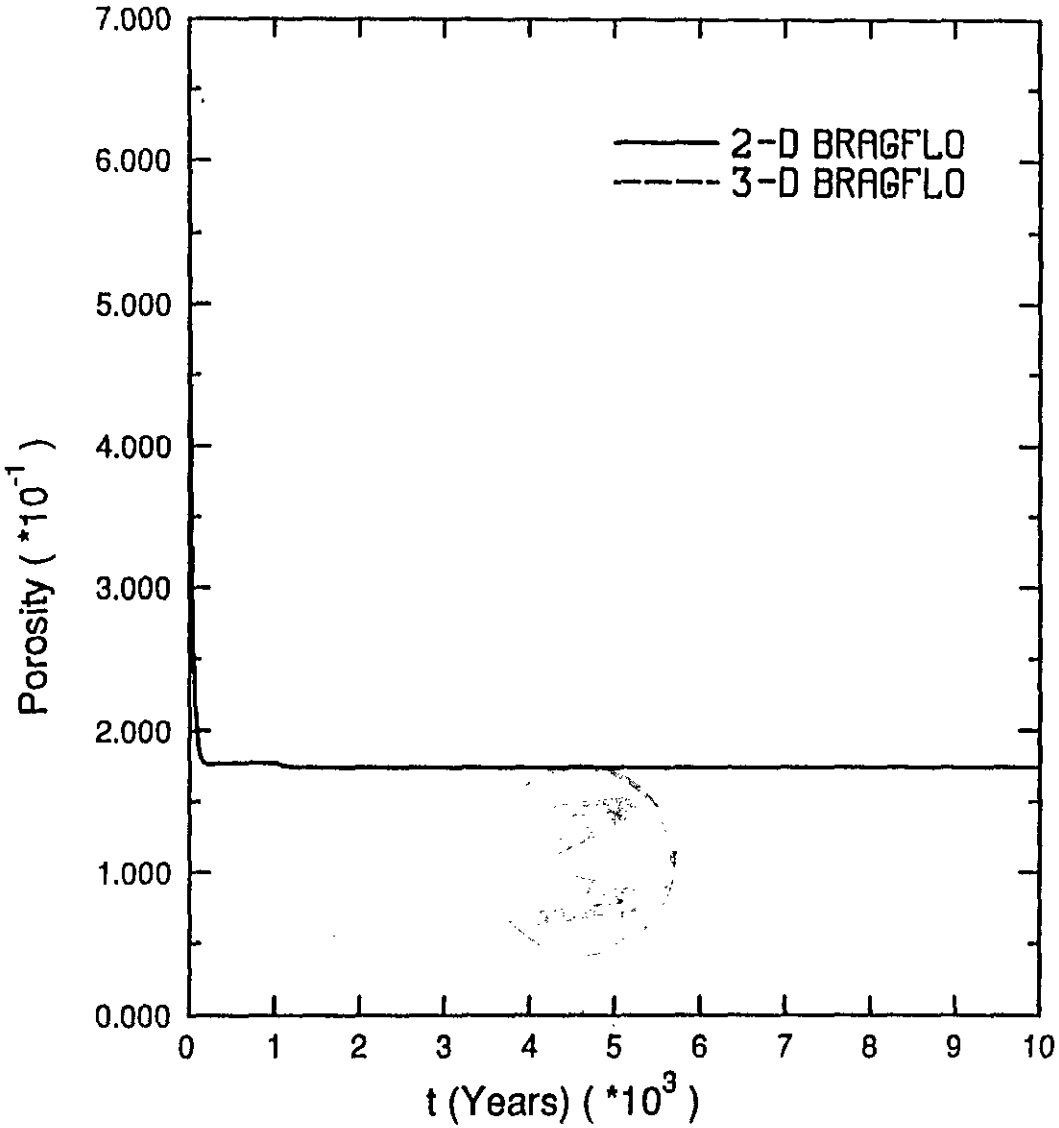

Fig. 13 Average Porosity In Repository - Doubled Gas Generation rate

SPLAT X2.0 01/24/96 18:47:39

ERRATA 2-14-96

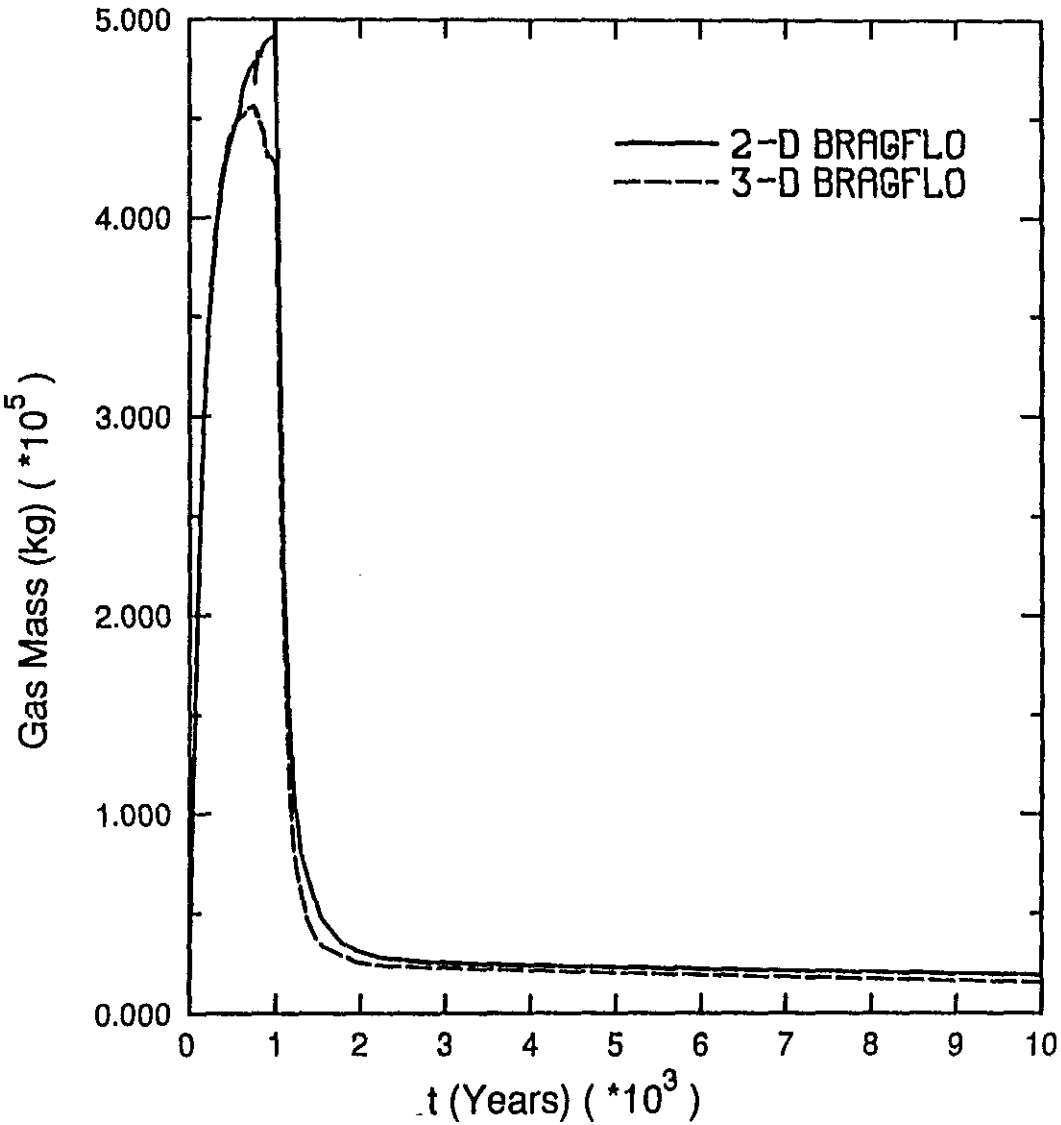

Fig. 14 Gas Mass in Place in Repository - Doubled Gas Generation rate

SPLAT X2.0 01/24/98 16:58:22

ERRATA 2-19-96

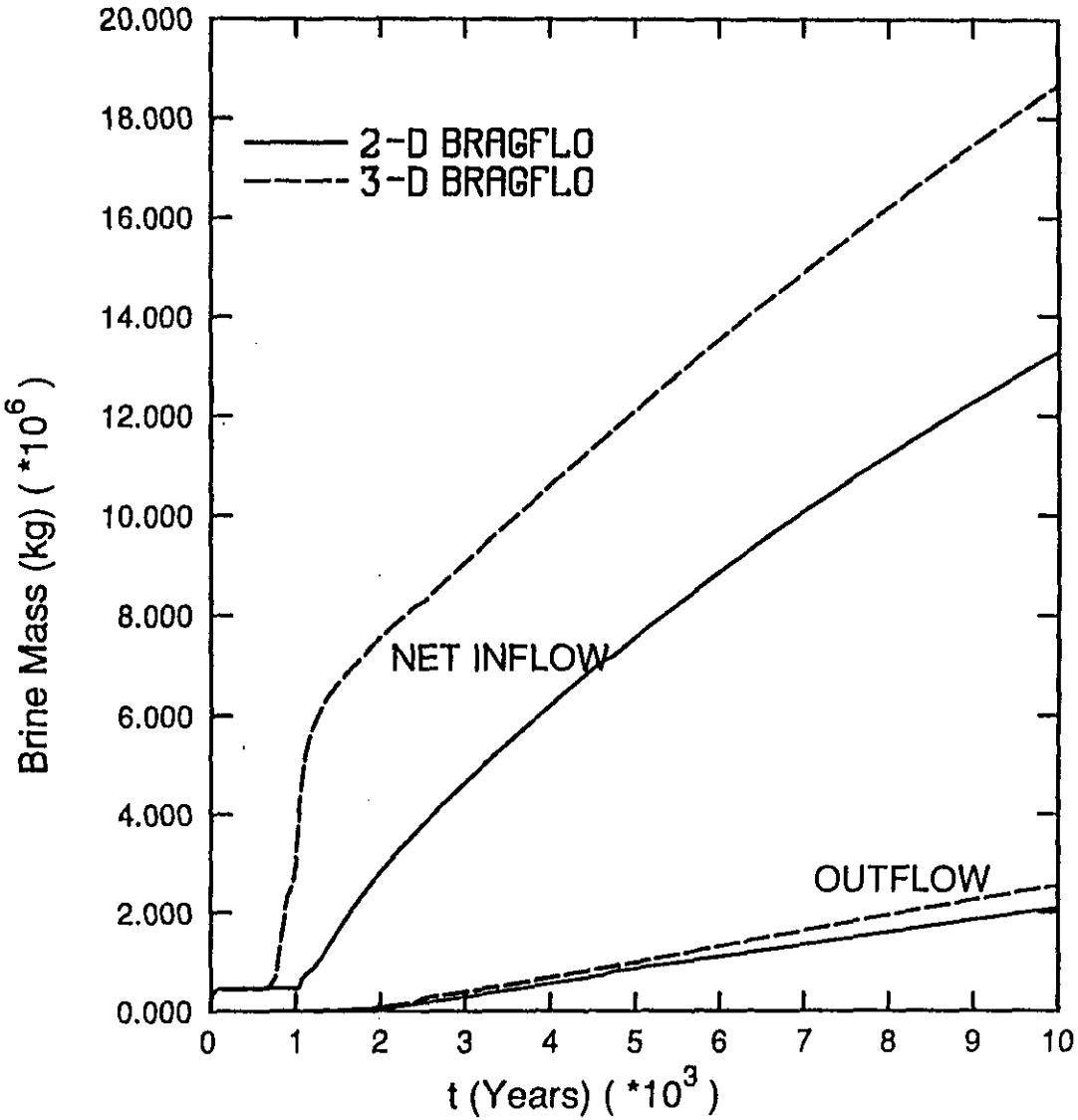

Fig. 15 Cumulative Net Brine In and Outflow at Repo.-Doubled Gas Generation rate

SPLAT X2.0 02/01/96 16:36:15

ERRATA
2-19-96

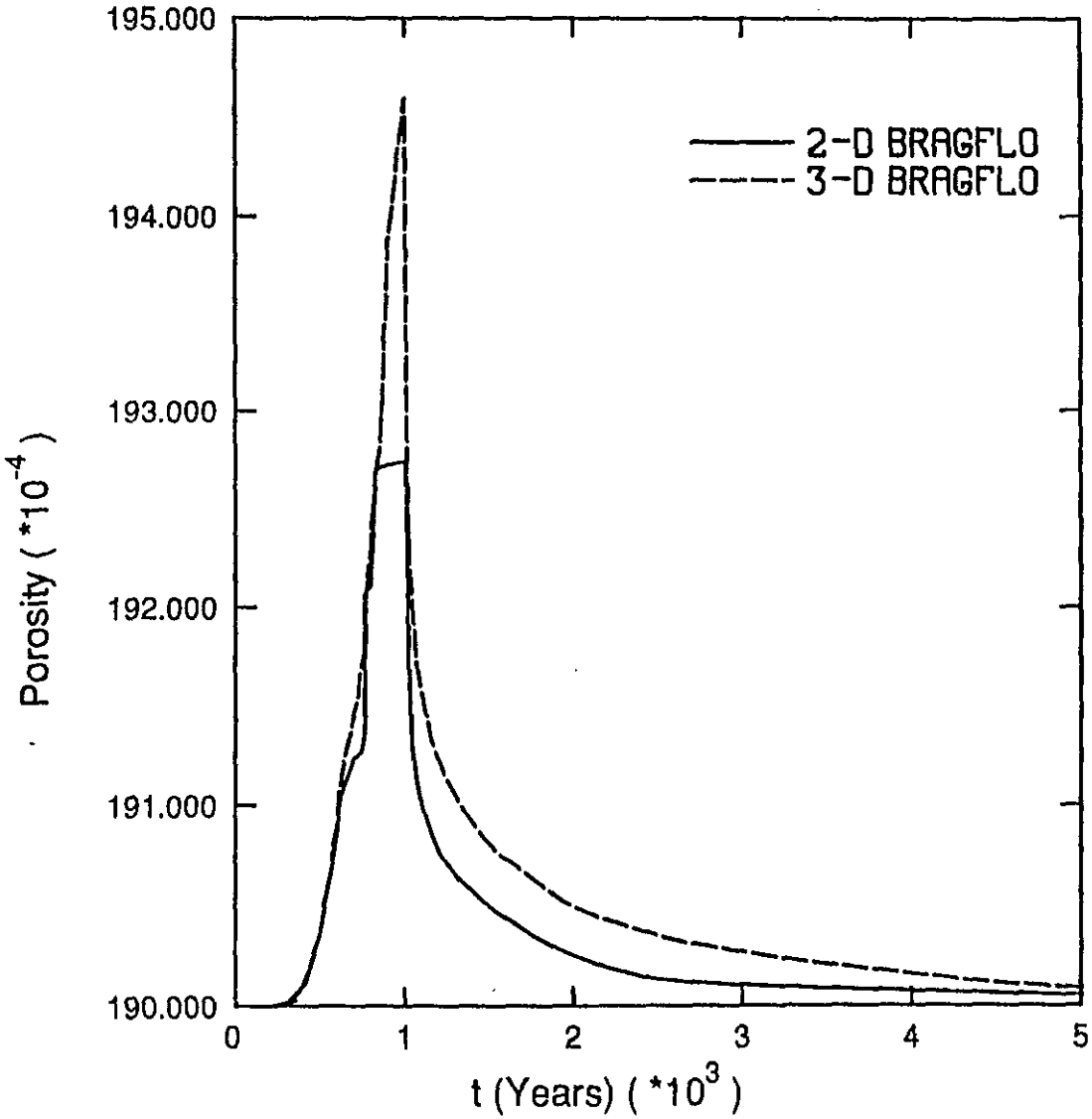

Fig. 16 Average Porosity in Anhydrite Layers - Doubled Gas Generation rate

F1:[FEP.THADGU.3DDBL_SPLAT]ANHDBLPORAVG.CMD;11

SPLAT X2.0 02/14/96 14:17:29

ERRATA 2-19-96